Available online at www.worldnewsnaturalsciences.com

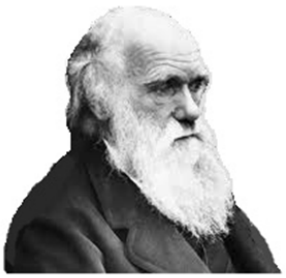

World News of Natural Sciences

An International Scientific Journal

WNOFNS 18(2) (2018) 79-105 EISSN 2543-5426

Integration of Aeromagnetic Data and Landsat Imagery for Structural Analysis: A Case Study of Awgu in Enugu State, South-Eastern, Nigeria

B. I. Ijeh, H. E. Ohaegbuchu* and **P. C. Okpetue**

Department of Physics, College of Physical and Applied Sciences,
Michael Okpara University of Agriculture, Umudike, Nigeria

*E-mail address: eo.henry@mouau.edu.ng

Tel: +2348132954367

ABSTRACT

In this study, digital format data comprising of aeromagnetic and remotely sensed (Landsat ETM+7) data were used for structural interpretation of the Awgu area (predominantly underlain by sedimentary rocks) in Enugu State, southeastern part of Nigeria. Aeromagnetic data were analyzed using the Oasis Montaj 7.5 software and interpretation was carried out by applying the vertical and horizontal gradients, analytical signal, reduction to pole, tilt depth, as well as Euler deconvolution. The total magnetic intensity map shows a magnetic signature ranging from -39nT to 129nT. The 3D Euler solution of the study area has a structural index of 1.0 with dyke/fault as the shape of the inferred geological structure. In the Landsat ETM+7 satellite data used, band 5 was found as the most suitable in (automatic) delineation. The automatic lineament extraction process was carried out utilizing the line module of PCI Geomatica (2015 version). The essence of analysis and interpretation of the Landsat ETM+7 was to determine the lineament trends and density across the area. Rockworks 16 version software was used to generate the rose diagrams. As a result of the work, the aeromagnetic and Landsat lineament maps of the study area were summarized using rose diagrams. This revealed NE-SW as the major trend with some secondary trends NW-SE, E-W and N-S directions. However, the NE-SW trend reflects the younger tectonic events, because the younger events are more pronounced and tend to obliterate the older events. In a comparison of the aeromagnetic and Landsat lineament extraction of the study area in terms of number of lineaments, directions and total length of lineaments, the Landsat imagery were found to be better than the number, directions and total length of the aeromagnetic data.

***Keywords*:** Aeromagnetic data, remote sensing, Landsat, structural analysis, Awgu

(Received 12 March 2018; Accepted 27 March 2018; Date of Publication 28 March 2018)

1. INTRODUCTION

1. 1. Aeromagnetic Survey

Aeromagnetic survey is a common type of geophysical survey which is carried out using a magnetometer aboard or towed behind an aircraft (Burger *et al*., 2006). The principle is similar to a magnetic survey carried out with a hand-held magnetometer, but allows much larger areas of the Earth's surface to be covered quickly for regional reconnaissance. The aircraft typically flies in a grid-like pattern with height and line spacing determining the resolution of the data (and cost of the survey per unit area). As the aircraft flies, the magnetometer measures and records the total intensity of the magnetic field at the sensor, which is a combination of the desired magnetic field generated in the Earth as well as tiny variations due to the temporal effects of the constantly varying solar wind and the magnetic field of the survey aircraft. By subtracting the solar, regional, and aircraft effects, the resulting aeromagnetic map shows the spatial distribution and relative abundance of magnetic minerals (most commonly the iron oxide mineral magnetite) in the upper levels of the Earth's crust. Because different rock types differ in their content of magnetic minerals, the magnetic map allows a visualization of the geological structure of the upper crust in the subsurface, particularly the spatial geometry of bodies of rock and the presence of faults and folds. This is particularly useful where bedrock is obscured by surface sand, soil or water. Aeromagnetic data was once presented as contour plots, but now is more commonly expressed as thematic (colored) and shaded computer generated pseudo-topography images. The apparent hills, ridges and valleys are referred to as aeromagnetic anomalies. A geophysicist can use mathematical modeling to infer the shape, depth and properties of the rock bodies responsible for the anomalies (Burger *et al*., 2006).

Magnetic method is one of the most economical geophysical techniques to delineate the subsurface structures (Sultan and Josef 2014). Generally, aeromagnetic anomaly maps reflect the lateral variations in the earth's magnetic field (Burger *et al*., 2006). These variations are related to changes of structures, magnetic susceptibility or remanent magnetization. It was observed that sedimentary rocks have low magnetic properties compared to metamorphic and igneous rocks, which have greater magnetic properties (intensity and susceptibility). Therefore airborne magnetic surveys are useful to map geologic structure on or inside the basement rocks or to detect magnetic minerals directly. Airborne geophysical surveys are an extremely important aspect of modern geophysics. Compared with ground surveys, airborne surveys allow faster and usually cheaper coverage, of large areas (Olowofela *et al*., 2012).

1. 2. Landsat Imagery

The Landsat program is the longest running enterprise for acquisition of satellite imagery of Earth. On July 23, 1972 the Earth Resources Technology Satellite was launched. This was eventually renamed to Landsat. The most recent, Landsat 8, was launched on February 11, 2013. The instruments on the Landsat satellites have acquired millions of images. The images, archived in the United States and at Landsat receiving stations around the world, are a unique resource for global change research and applications in agriculture, cartography, geology, forestry, regional planning, surveillance and education, and can be viewed through the USGS 'EarthExplorer' website. Landsat 7 data has eight spectral bands with spatial resolutions ranging from 15 to 60 meters; the temporal resolution is 16 days (Opara *et al*., 2012).

Landsat imagery is relatively high resolution earth observation data that is acquired through sensors on one of the NASA Landsat satellites. The satellite sensors acquire high integrity images of the planet surface in a systematic fashion. Users can take this imagery and use it to determine the health and type of vegetation, amount of built surfaces, success of agriculture or apply it for myriad other uses.

The use of satellite imagery for regional mapping of geologic units and structures has long been demonstrated as a vital tool for regional geologic mapping. This is as result of its ease of operation, speed, accuracy, low cost and coverage. In addition, advancements lately in satellite and digital technologies have led to remarkable improvement in this technique (Onyewuchi, et al., 2012).

1. 3. Lineaments

A lineament is a linear feature in a landscape which is an expression of an underlying geological structure such as a fault. Typically a lineament will comprise a fault-aligned valley, a series of fault or fold-aligned hills, a straight coastline or indeed a combination of these features (Whitten and Brooks, 1972; Attoh and Brown 2008). Fracture zones, shear zones and igneous intrusions such as dykes can also give rise to lineaments. Other causes of lineaments include roads and railroads, contrast-emphasized contacts between natural or man-made geographic features (e.g., fence lines), or vague "false alarms" caused by unknown (unspecified) factors. The human eye tends to single out both genuine and spurious linear features, so that some thought to be geological may, in fact, be of other origins. Lineaments are often apparent in geological or topographic maps and can appear obvious on aerial or satellite photographs. Lineaments have also been identified on other planets and their moons. Their origins may be radically different from those of terrestrial lineaments due to the differing tectonic processes involved (Ananaba, 1991; O'Leary *et al.*, 1976).

2. LOCATION OF THE STUDY AREA

The study was carried out in Awgu area of Enugu State, South-Eastern, Nigeria. Awgu area is located within latitude 6°01' N to 6°10' N and longitude 7°26' E to 7°38' E. Enugu state is bounded by Anambra in the west, Benue in the North-east, Kogi in the North- west, Imo in the South and Ebonyi in the East. It has accessible roads and major rivers which are clearly indicated in Figure 1

3. DATA ACQUISITION: AEROMAGNETIC STUDY AND LANDSAT IMAGERY

The aeromagnetic map was acquired from National Geological Survey Agency (NGSA), Abuja. A high resolution airborne magnetic data of Nkalagu sheet 302 on a scale of 1:100,000 from Nigeria Geological Survey Agency was used. The survey parameters of the aeromagnetic data are: Flight line spacing (500 m), Tie line spacing (2 km), Terrain clearance (80 m), Flight direction is NW-SE while the Tie line direction NE-SW. The original Total Magnetic Intensity (TMI) was processed, filtered and transformed to other grids using Oasis Montaj 7.5 software with associated extensions of the package such as MAGMAP, CET such as the first and second vertical derivatives, horizontal gradient, Analytical signal, Reduction to

pole, tilt depth, Euler deconvolution. ArcGIS software by ESRI was used to relate and overlay various layers of information, such as geology, magnetic data and extract structural features of the interpretation. The interpretation was performed on screen in the ArcMap. Quality hardcopy results were produced directly from ArcMap.

The Landsat imagery was downloaded from GLCF- Global Land Facility Cover website using the co-ordinates 6°01' N - 6°10' N latitudes and longitudes 7°26' E - 7°38' E, that covers the area. The automatic lineament delineation was based on decision of the most appropriate band for edge enhancement, followed by edge sharpening enhancement technique which gives the best result of lineaments that are not delineated by human eyes, and apply LINE module of PCI Geomatica 2015 for recognized lineaments. Landsat ETM+7 satellite data were used and the first step was to select the band that should be used for lineament extraction (Süzen and Toprak, 1998; Madani 2001). Visual inspection of the individual bands was carried out, based on the ability to identify features, and band 5 was selected and it was stretched linearly to output range. The second step was to select the filter type. For this purpose, different types of filters were tested. Edge sharpening enhancement filter was the best which convolved over band 5. Edge sharpening enhancements make the shapes and details for analyses. Edge sharpening was applied using PCI Geomatica 2015 software package. And finally the final image of the study area was used for automatic lineament extraction. The lineament extraction algorithm of PCI Geomatica software consists of edge detection, thresholding and curve extraction steps. After the extraction of the lineaments, the orientation of each lineament was calculated and a Rose Diagram which explains the frequency of lineation in a given orientation was plotted using Rockworks 16 software to generate the rose diagram.

4. DATA INTERPRETATION

Interpretation methodology consists of inspection of computer screen, hard-copy images, and maps of the aeromagnetic data to define the various observable structures. Structures can be recognized by Offsets of apparently similar magnetic units, sudden discontinuities of magnetic units, and an abrupt change in depth to magnetic sources.

5. RESULTS AND DISCUSSIONS

5. 1. Total Aeromagnetic Intensity Map

Figure 2 is the total magnetic intensity field over Awgu area on a scale of 1:75,000, showing a magnetic signature ranging from -39nT - 129nT, the contour interval is 20nT. The magnetic high of magnitude 129nT is observed in some part of northwestern part of the study area. The colour patterns represent total magnetic intensity and can be used to interpret lithology, alteration, and structure in the survey area. The closely spaced contours from northwestern and southwestern part of the study area suggests the possibility of faults or local fractured zones passing through these areas.

The visual inspection of the aeromagnetic map shows that the contour lines of northwestern and southwestern parts are closely spaced indicating that the depth to basement is shallow in these areas. The northeastern and southeastern parts are widely spaced indicating

that the depth to magnetic basement is relatively high when compared to those of the northwestern and southwestern parts.

According to Usman, 2012, a positive magnetic anomaly is a reading of magnetic field strength that is higher than the regional average which can indicate hidden ore and geologic structures. This positive magnetic contour reading is found in the northwestern part of the study area, while a negative magnetic anomaly is a reading of magnetic field strength that is lower than the regional average, this is found in the southwestern part of the study area.

5. 2. Vertical Derivative (Gradient)

Vertical gradients of magnetic fields represent magnetic fields in which regional effects and interference between adjacent anomalies have been suppressed. The vertical derivative is physically equivalent to measuring the magnetic field simultaneously at two points vertically above each other, subtracting the data and dividing the result by the vertical spatial separation of the measurement points (Labbo and Ugodulunwa, 2007). The computation of vertical gradients is analogous to the application of a high pass filter. The Vertical derivative (gradient) operator is often applied to ground or airborne magnetic data to sharpen the edges of anomalies, enhance shallow features and other significant features. The algorithm is given by (Gunn 1975, Hani *et al*., 2013) as:

$$A(u,v) = A(u,v)\,[(u^2 + v^2)^{0.5}/n]^n \quad (1)$$

where: ***A(u,v)*** is the amplitude present at those frequencies, and ***n*** is the order of derivative. The higher the order of derivative, the noisier the map will become.

5. 2. 1. First Vertical Derivative

First vertical derivative (Figure 3) enhance shallow features. It is potentially less sensitive to noise in the data compared to methods relying on higher order derivatives.

5. 2. 2. Second Vertical Derivative Map

Second vertical derivative (Figure 4a) is the vertical gradient of the first vertical derivative. It enhances shallower anomalies. The frequency response formula of these operations shows that the process enhances high frequencies relative to low frequencies and this property is the basis for the application of the derivatives processes to eliminate long-wavelength regional effects and resolve the effects of the adjacent anomalies (Gunn and Milligan, 1997). Apart from enhancing the shallower anomalies the second vertical derivatives are also used to delineate geological boundaries between rocks with contrast in physical properties such as magnetic susceptibility. The contoured second vertical derivative (Figure 4b) outlines the bodies causing the magnetic anomalies. These filters are considered most useful for defining the edges of bodies and for amplifying fault trends. In mathematical terms, a vertical derivative can be shown to be a measure of the curvature of the potential field, while zero second vertical derivative contours defines the edge of the causative body. Thus, the second vertical derivative is in effect a measure of the curvature, i.e., the rate of change of non- linear magnetic gradients.

5. 3. Horizontal Gradient

Figure 5 is the horizontal gradient (HG). It is considered as the simplest approach to estimating contact locations (e.g. faults). It displays detailed information about the structures, contacts and the tectonic setting of the study area.

Horizontal gradient filtering is especially useful for approximating the horizontal location of magnetic edges and for estimating maximum and minimum source depths. Another advantage of using this method is that it produces relatively coherent results that are insensitive to noise, which aids in interpreting the solutions (Phillips and Grauch, 2001). One drawback of horizontal gradient filtering is that it can produce identical results for vertical magnetic contacts as for a number of other geologic features such as homoclines, high-relief topography, and igneous lithologic contacts (Grauch *et al*., 2009). Additionally, it is often difficult to effectively use horizontal gradient filtering if the data has not been filtered to remove long wavelength components of the data, as their effect may distort the local features of interest (Grauch and Johnston, 2002)

5. 4. Analytical Signal

Analytic signal can sharpen and enhance regional structure and the edges of the anomalies in a grid. The analytic signal method is moderately sensitive to the noises in the data and to the interference effects between the nearby sources. Analytical signal (Figure 6) was calculated for the area which positions the anomaly at the centre of the causative body by combining both vertical and horizontal derivatives. Analytical signal is considered better enhancement technique since dipolar effects are absent and even for small bodies the peaks merge resulting to an anomaly cantered above the causative body. It is also observed that the vertical derivative applied to the analytical signal has sharpened up and positioned the anomaly more exactly than the original analytical signal image. An important characteristic of the analytical signal is that it is independent of the direction of the magnetization of the source. The amplitude of the analytical signal is also related to the amplitude of magnetization (Beamish, 2012). The analytical signal amplitude ranges from -0.016nT/m to 0.019nT/m thus, having a high amplitude around the northwest and low amplitude around the southwest part of the study area.

5. 5. Reduction to Pole

Reduction-to-Pole (RTP) - The reduction to pole filtering process removes the effect of the earth's magnetic field by way of a gross shift of the observed magnetic readings. The procedure is nothing more than a correction factor applied across the study area to remove the non-vertical magnetic component (causative body) in its correct spatial position. This process helps better define boundaries between different basement lithologies with different magnetic susceptibilities (David and Oliver, 1998). The reduction to pole (RTP) transformation (Figure 7) was applied to the aeromagnetic data to minimize polarity effects (Blakely, 1995). These effects are manifested as a shift of the main anomaly from the centre of the magnetic source and are due to the vector nature of the measured magnetic field. The RTP transformation usually involves an assumption that the total magnetizations of most rocks align parallel or anti-parallel to the Earth's main field.

5. 6. Tilt Depth

The Tilt angle, θ, is measured in either radians or degrees. Since the Tilt angle consists of the ratio of the vertical and horizontal derivatives, the resulting Tilt function, of the RTP field, does not contain information on the induced magnetization of the causative bodies, such that for a given body with induced magnetization, J_i, the tilt response will be the same whether the body is strongly or weakly magnetized. The advantage of the tilt-depth method is however its ability to identify those parts of anomaly structures that are least affected by interference where repeated depth estimates are most likely to be reliable (Salem *et al*., 2007). The depth and structural information contained within the tilt signal remain unaffected. The depth estimates can be derived directly from the tilt map legend with the North West and South east having a high depth of 1.311 to 1.567 km while showing the Southwest and northeast having a low depth of -1.551 to -1.257 km.

5. 7. Euler Deconvolution

Euler deconvolution is a method to estimate the depth of subsurface magnetic anomalies. It is particularly good at delineating the subsurface contacts. An Euler depth estimation increases with N and real bodies are simulated by superposition of bodies. Structural index which is a measure of the rate of change with distance of a field (John and Emmanuel 2014) and directly relates to the shape of the source of the field (Raimi *et al.*, 2014). An index that is too low gives depths that are too shallow; one that is too high gives estimates that are too deep.

The structural index (Figure 9) for the study area is 1.0 giving the shape of the inferred geological structure as a dyke/fault. The structural features of the study area has a maximum depth of 756.103 m and a minimum depth of -407.255 m.

5. 8. Aeromagnetic Lineament Map

Magnetic lineaments reveals a wealth of structural detail. The aeromagnetic lineament map (Figure 10) shows several lineaments trending in the northeast-southwest directions. There are concentration of lineaments on the northeastern and southwestern part of the lineament map while on the northwestern and southwestern part is less concentrated. There are three major faults on the map.

5. 9. Landsat Imagery

Edge enhancement filters were applied to the image using the Radar Interpreter tool of Erdas Imagine Software. The Prewitt Gradient filter was applied in this case, using 5 different directions such as North filter, South filter, West filter, East filter, Non-directional filter. The filtered images were then used for the extraction of lineaments which were then merged together. After the extraction of the lineaments (Figure 11a, 11b, 11c and 11d), the orientation of each lineament was calculated and a Rose Diagram (Figure 12) which explains the frequency of lineation in a given orientation was plotted.

The lineament density map shows that lineament density is high around the southwestern part of the study area. Lineament density map was generated in order to highlight areas with high prevalence of structures. The orientations of extracted Landsat lineaments as in (Figure 12) were created by using rose diagram.

The total number of lineaments is 313, the total length of all lineations is 626 km, and the maximum bin length is 29 km. The major trend of lineaments is NE-SW while the minor trend of lineaments are NW-SE, E-W and N-S directions. Likewise, the orientations of extracted aeromagnetic lineaments as in (Figure 12b) were created by using rose diagram. The total number of lineaments is 211, the total length of all lineations is 422 km, and the maximum bin length is 75 km. The major trend of lineaments is NE-SW while the minor trend s of lineaments are NNE-SSW directions.

6. CONCLUSIONS

The aeromagnetic and Landsat data were subjected to various image and data enhancement and maps were generated such as the total magnetic intensity, vertical derivatives - first and second derivatives, horizontal gradient, analytical signal, Reduction to pole, tilt depth, Euler deconvolution, aeromagnetic lineaments map, Landsat lineaments map, lineament density map and rose diagrams. The total magnetic intensity over Awgu after digitization showed a magnetic signature ranging from -39nT to 129nT.

Lineament analysis is a valuable source of information for studying the structural setting of an area, it helps to reveal zones of fracture concentration and identification of surface features. Linear features as seen on satellite images are usually the results of aligned morphologic rock or topographic relief of the basement. The aeromagnetic and Landsat lineament maps of the study area have been summarized using rose diagrams, revealing NE-SW as the major trend with some secondary trends NW-SE, E-W and N-S directions. However, the NE-SW trend reflects the younger tectonic events, because the younger events are more pronounced and tends to obliterate the older events. In comparison of the aeromagnetic and Landsat lineament extraction of the study area in terms of number of lineaments, directions and total length of lineaments; the number, directions and total length of the Landsat imagery were found to be more than the number, directions and total length of the aeromagnetic data.

The lineament trends correspond to faults, geologic boundaries, folds and tectonically related joints in the area causing the ruggedness of the topography of the south-eastern Nigeria which had been interpreted to be a basin associated with two major fault lines trending NE – SW and NW – SE. The area has a dendritic drainage pattern which is structurally controlled.

This present research is therefore in agreement with previous studies which suggested that Nigeria has a complex network of fractures and lineaments with dominant trends of NW-SE, NE-SW, N-S and E-W directions. These linear structures running NE-SW observed from the study are suggested as the continental extension of the known pre-cretaceous oceanic fracture zones. Charcot and Chain fracture zones which run along the trough axis beneath the edimentary cover.

References

[1] Ananaba, S.E. (1991). Dam sites and crustal megalineaments in Nigeria. *ICT Journal* 1: 26-29.

[2] Attoh, K., Brown, L.D. (2008). The Neoproterozoic Trans-Saharan/Trans-Brasiliano shear Zones: Suggested Tibetan Analogs. American Geophysical Union.

[3] Beamish, D. (2012). The application of spatial derivatives to non-potential field data Interpretation. *Geophysical Prospecting.* 60, 337-360.

[4] Blakely, R.J. (1995). Potential theory in gravity and magnetic applications. Cambridge University Press, Australia. 6: 116-139.

[5] Burger R.H., Sheehan, A.F., Jones, C.H. (2006). Introduction to Applied Geophysics Published by W.W. Norton. 600 pages.

[6] David, L.C. and Oliver N.M. (1998). Aeromagnetic demonstration survey with basement Interpretation and deep structure mapping. Final report prepared for the New York State Energy Research and Development Authority. 1-20.

[7] Grauch, V. J. S. and Johnston, C. A. (2002). Gradient window method: A simple way to Separate regional from local horizontal gradients in gridded potential-field data, 2002 Technical Program Expanded Abstracts, 72nd Annual Meeting, Society of Exploration Geophysicists 762-765.

[8] Gunn P.J. (1975). Linear transformation of gravity and magnetic fields. *Geophysical Prospecting* 23(2). 300-312.

[9] Gunn, P.J., Maidment D. and Milligan, P.R. (1997). Interpreting aeromagnetic data in areas of limited outcrop. *AGSO Journal of Australian geology and geophysics* 17(2), 175-185.

[10] Hani A., Nezar, H., Mohammed, A., Elias, S., Abdullah, D., Mohammed, H. and Rida, A. (2013). Integration of aeromagnetic data and landsat imagery for structural analysis purposes: A case study in the southern part of Jordan. *Journal of geographic information system.* 5, 198-207.

[11] John, M.U. and Emmanuel U.E. (2014). Structural analysis using aeromagnetic data: Case study of parts of southern Bida basin, Nigeria and the surrounding basement rocks. *Earth Science Research.* 3(2), 27-42.

[12] Labbo, A.Z. and Ugodulunwa F.X.O. (2007). An interpretation of total intensity aeromagnetic maps of part of southeastern Sokoto basin. *Journal of engineering and applied sciences* 3; 15-20.

[13] Madani, A.A (2001). Selection of the optimum landsat thematic mapper bands for automatic lineaments extraction, Wadi Natash area, Southeastern desert, Egypt. *Asian Journal of Geoinformatics.* 3(1), 71-76.

[14] O'Leary, D.W., Friedman J.D., and Phn, H.A. (1976). Lineament, Linear, Lineation: Some proposed new standards for old terms. *Geology Society American Bulletin* 87: 1463-1469.

[15] Olowofela, J.A., Akinyemi, O.D., Idowu, O.A., Olurin, O.T and Ganiyu S.A. (2012). Estimation of Magnetic Basement Depths beneath the Abeokuta Area, South west Nigeria from Aeromagnetic Data using Power Spectrum. *Asian Journal of Earth Sciences* 5(2), 70-78.

[16] Onyewuchi, R.A, Opara, A.I, Ahiarakwa, C.A and Oko, F.U. (2012). Geological Interptretations inferred from airborne magnetic and landsat data: Case study of Nkalagu area, southeastern, Nigeria. *International journal of science and technology* 2 (4), 178-191.

[17] Opara, A.I., Ugwu, S.A. and Onyewuchi R.A. (2012). Structural and tectonic interpretations from landsat 5 thematic imagery: case study of Okposi brine lake and environs, lower Benue trough, Nigeria. *Elixir Remote Sensing* 49, 9708-9713.

[18] Phillips, J. D. and Grauch, V. J. S. (2001). Some current research on the processing and interpretation of potential-field data at the U.S. Geological Survey, in Workshop on future directions in the analysis of potential-field data, August 18, 2001, Perth, Australia.

[19] Raimi, J., Dewu, B.B.M, Sule, P. (2014). An interpretation of structures from the Aeromagnetic field over a region in the Nigerian younger granite province. *International journal of geosciences* 5, 313-323.

[20] Salem, A., Williams, S., Fairhead, J.D., Smith, R., and Ravat, D. (2007). Tilt-depth method: A simple depth estimation method using first-order magnetic derivatives. *The Leading Edge*, 26(12), 1502-1505.

[21] Sultan, A.S.A and Josef, P. (2014). Delineating groundwater Aquifer and subsurface structures using Integrated Geophysical interpretation at the Western part of Gulf of Aqaba, Sinai, Egypt. *International Journal of Water Resources and Arid Environments* 3(1), 51-62.

[22] Suzen, M.L and Toprak, V. (1998). Filtering of satellite images in geological lineament analyses: An application to a fault zone in Central Turkey. *International journal of remote sensing* 19(6), 1101-1114.

[23] D G A Whitten with J R V Brooks (1972). The Penguin dictionary of Geology. Published by Allen Lane, London.

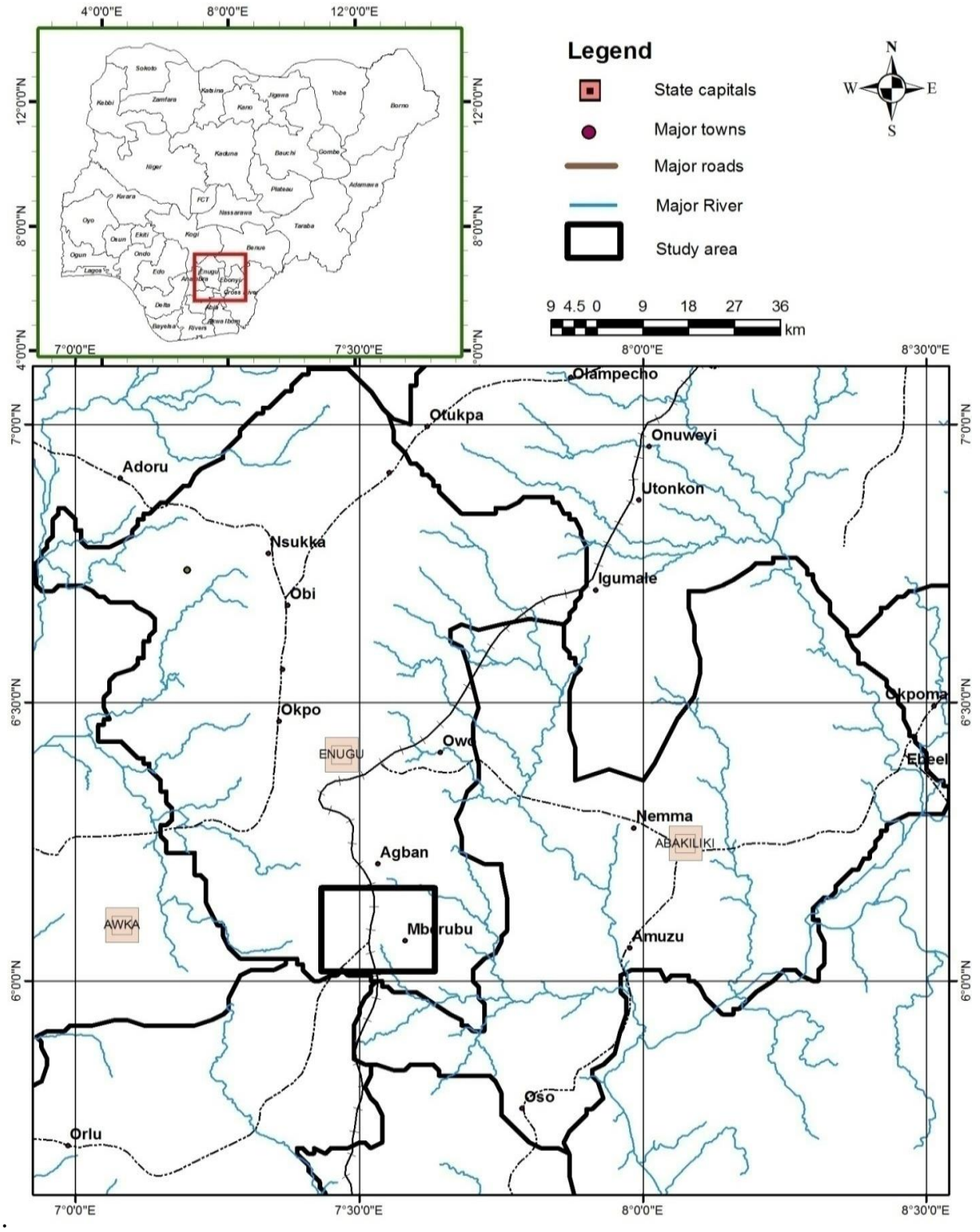

Figure 1. Location map of the study area.

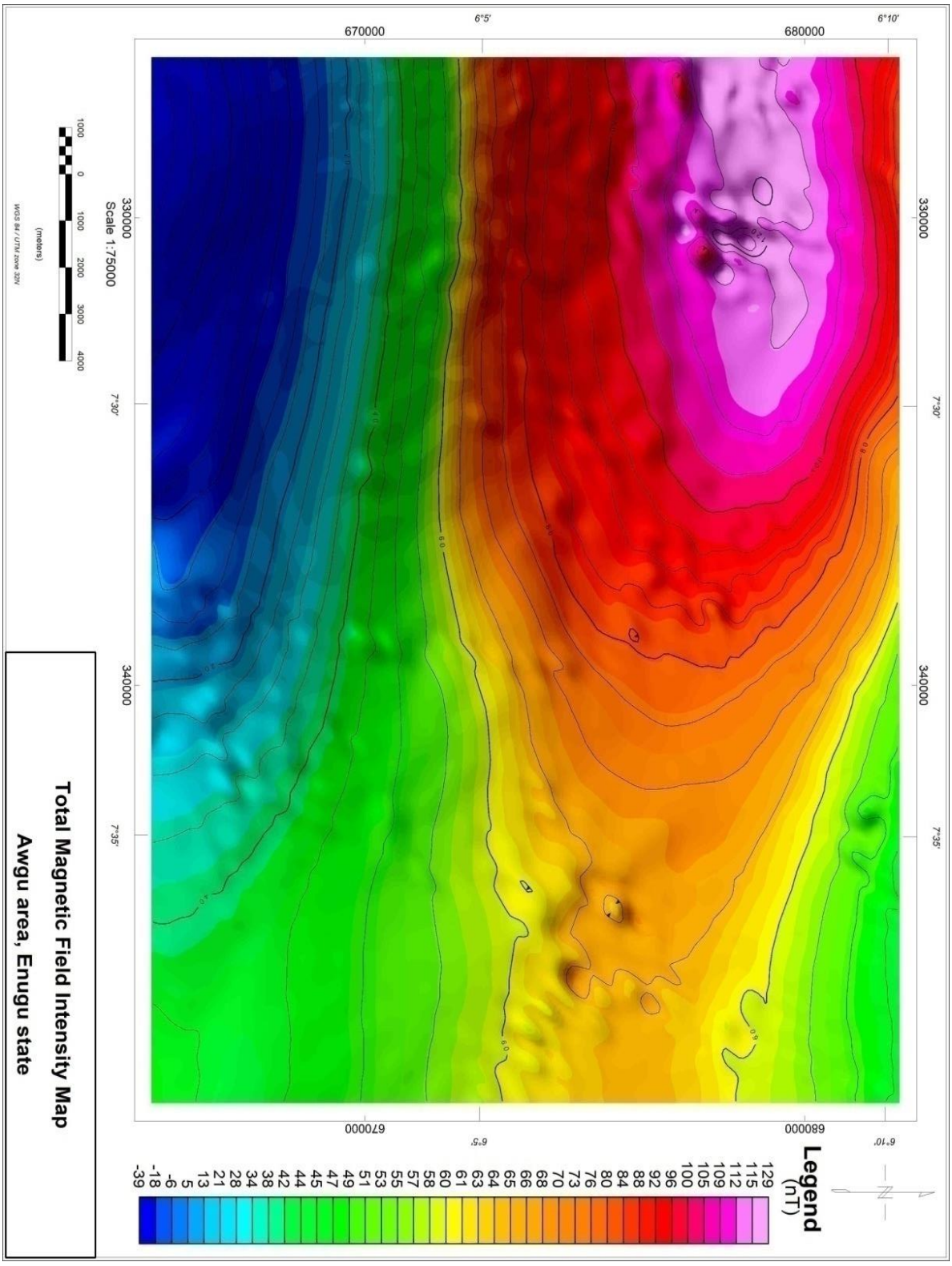

Figure 2. Total Magnetic Field Intensity Map of Awgu area.

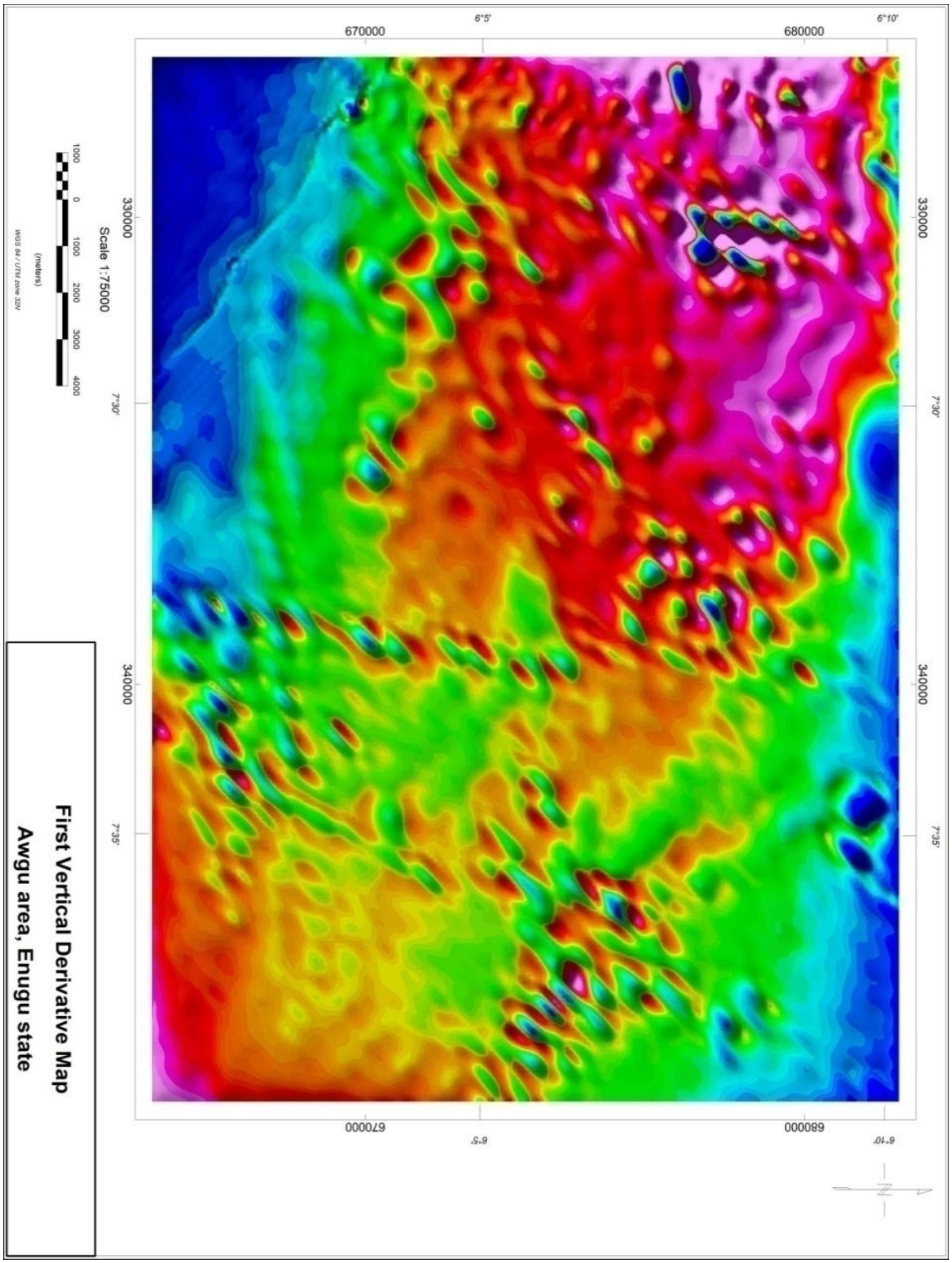

Figure 3. First vertical derivative map.

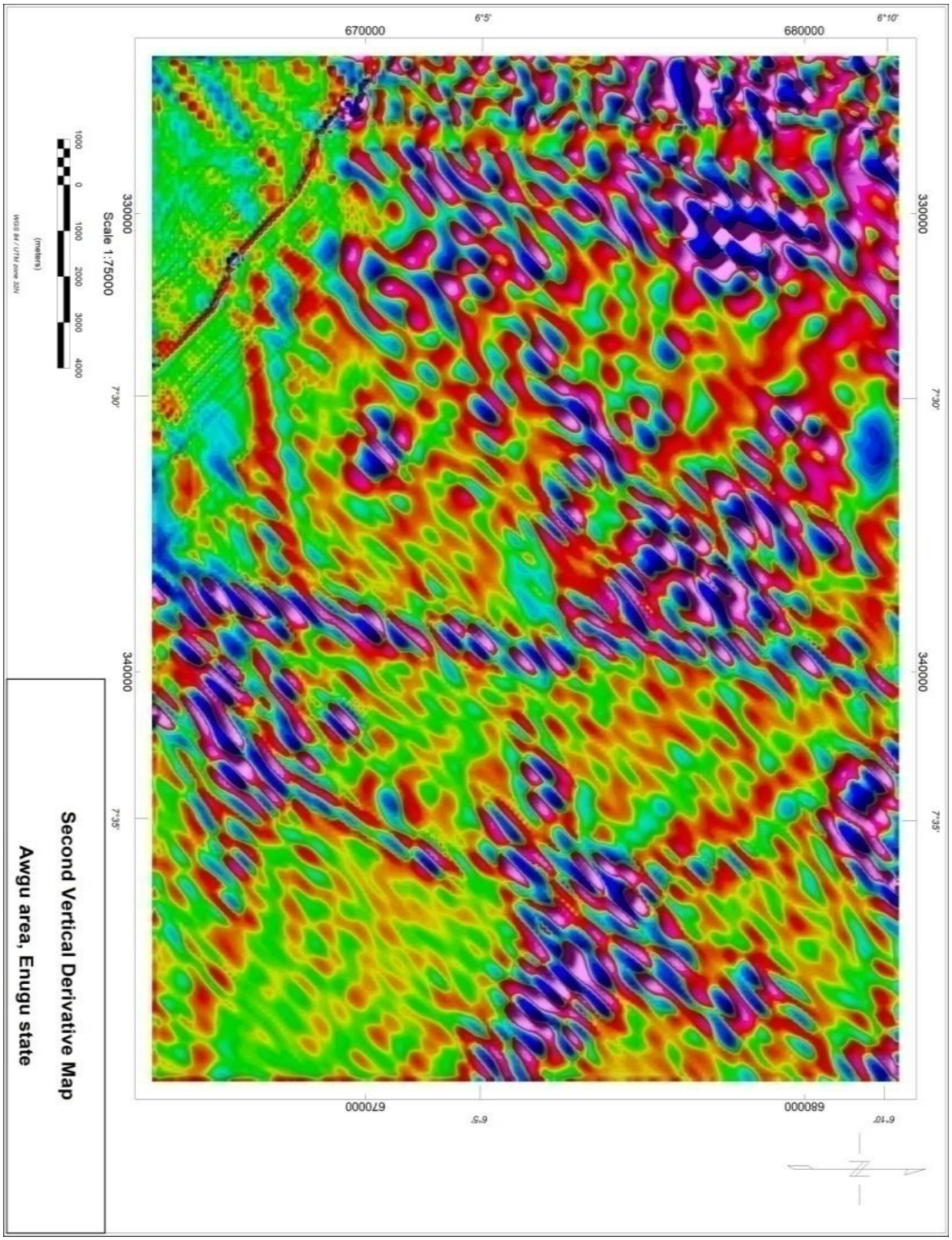

Figure 4a. Second vertical derivative map.

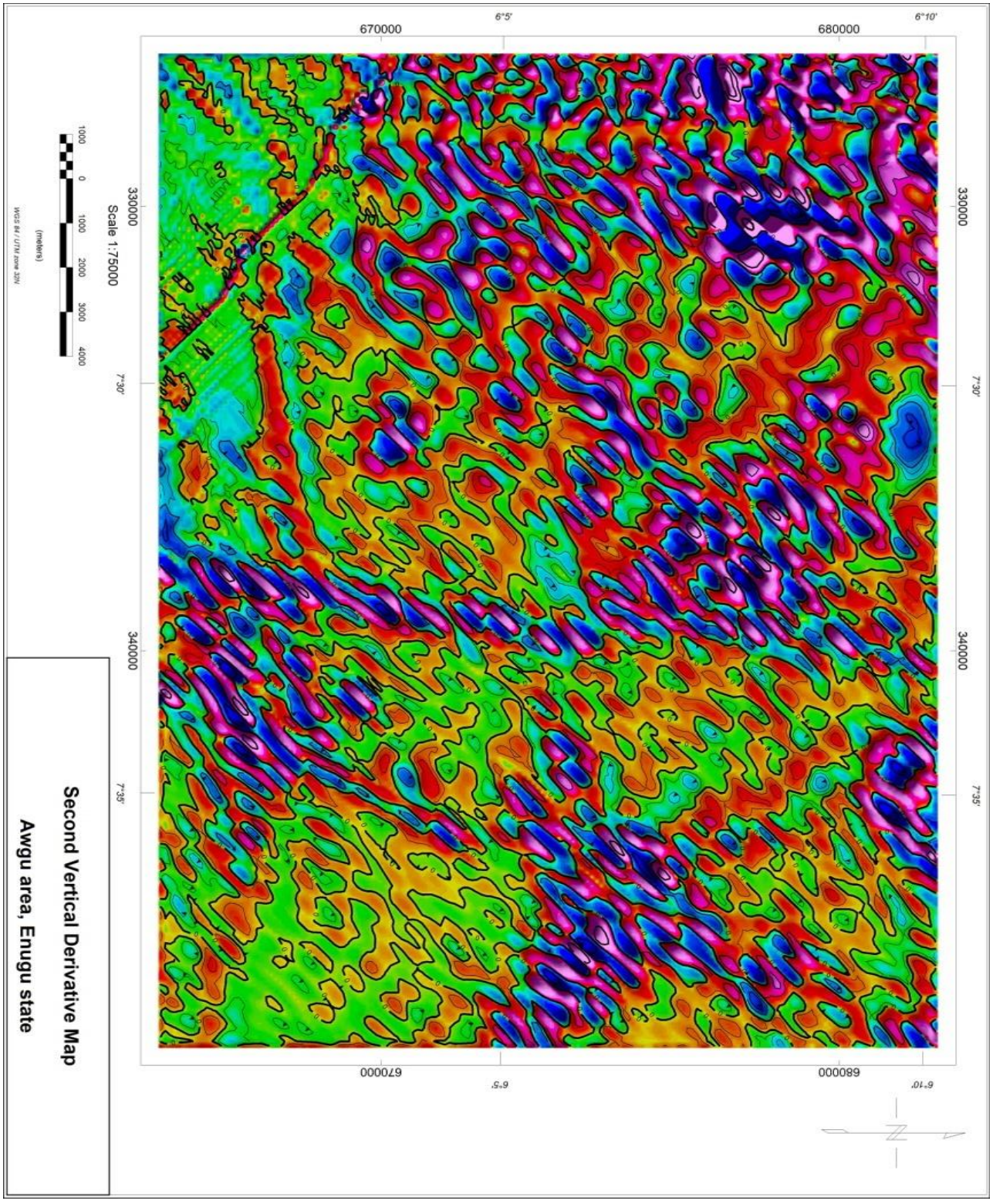

Figure 4b. Second vertical derivative contoured map.

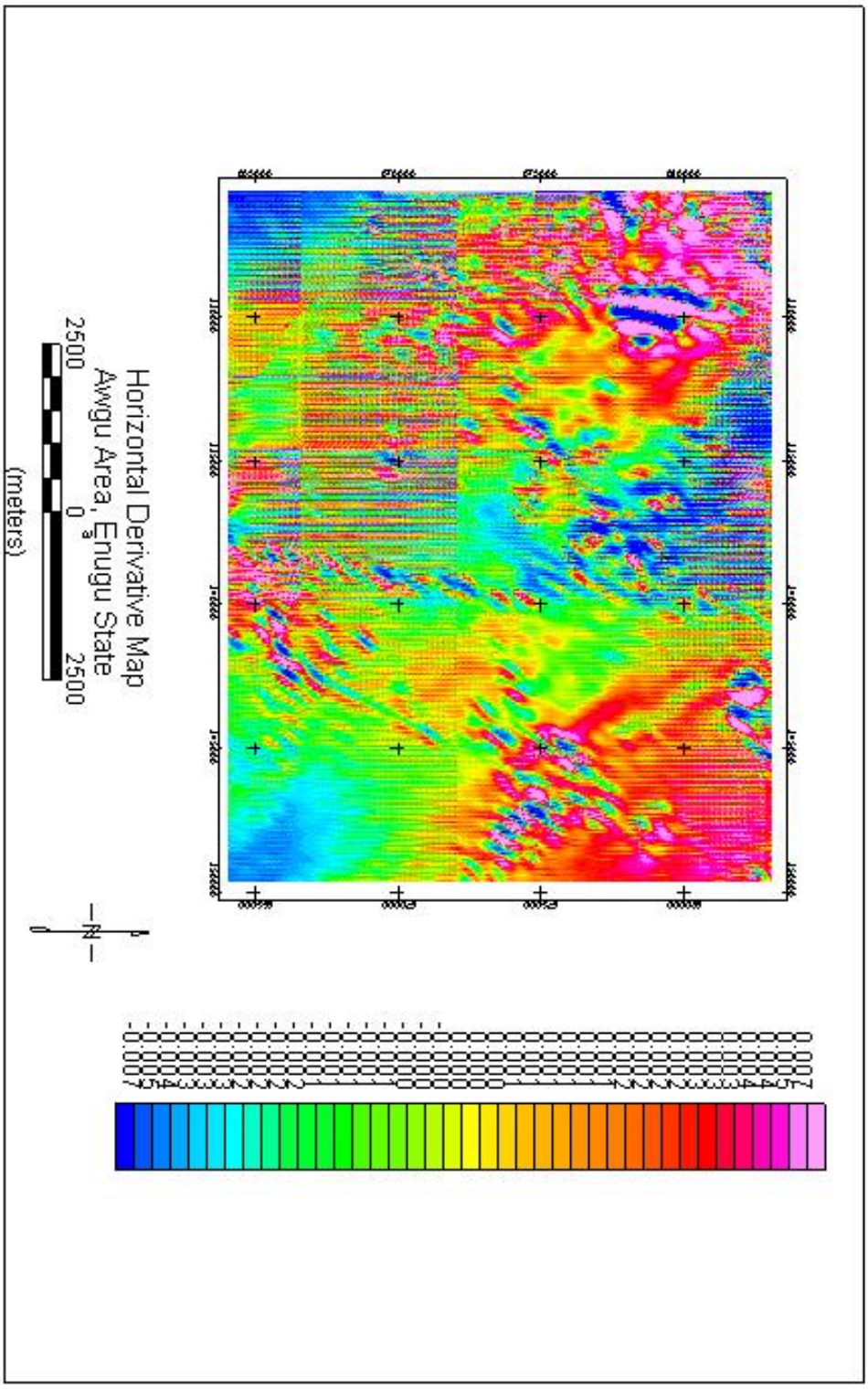

Figure 5. Horizontal derivative map.

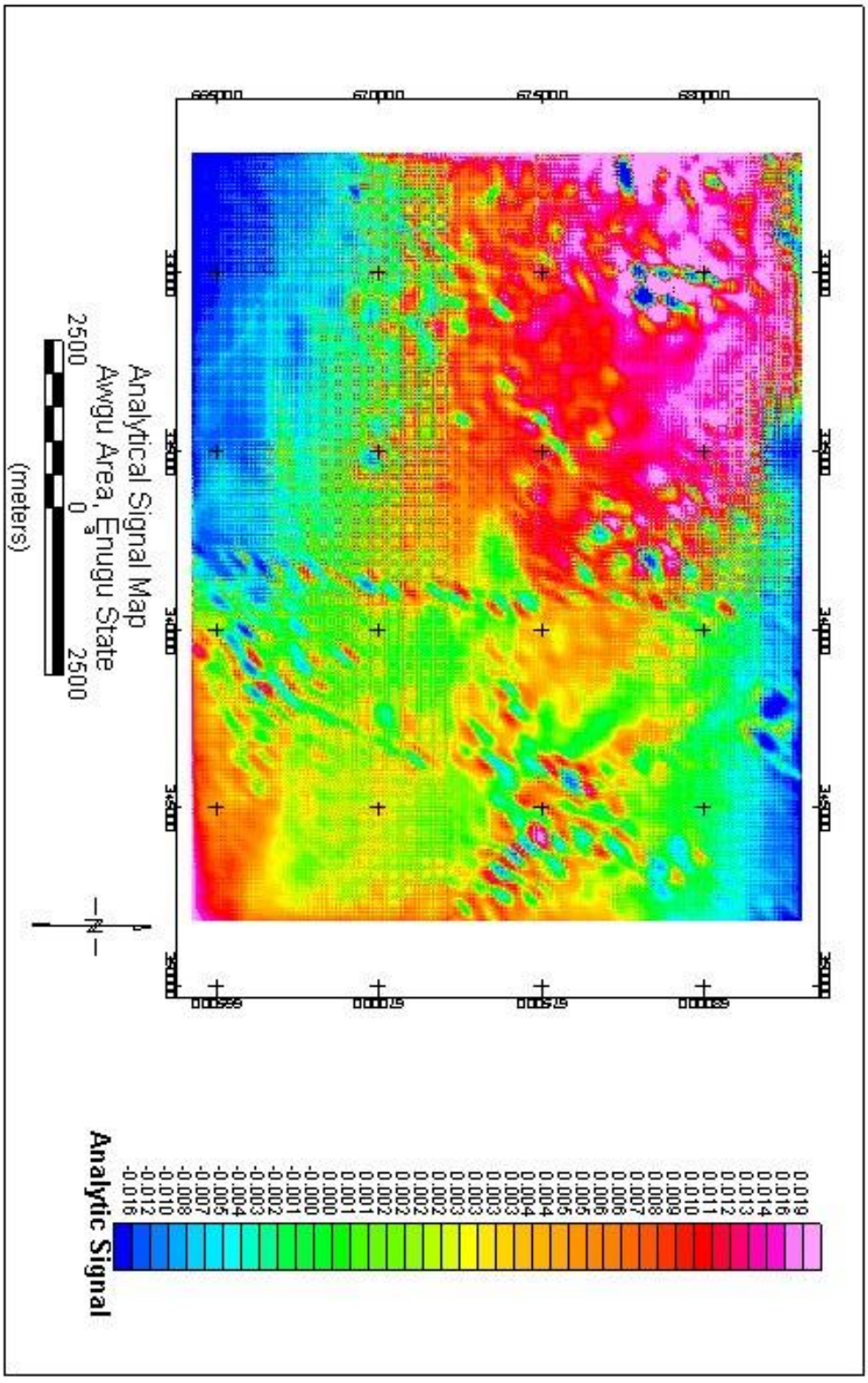

Figure 6. Analytical signal.

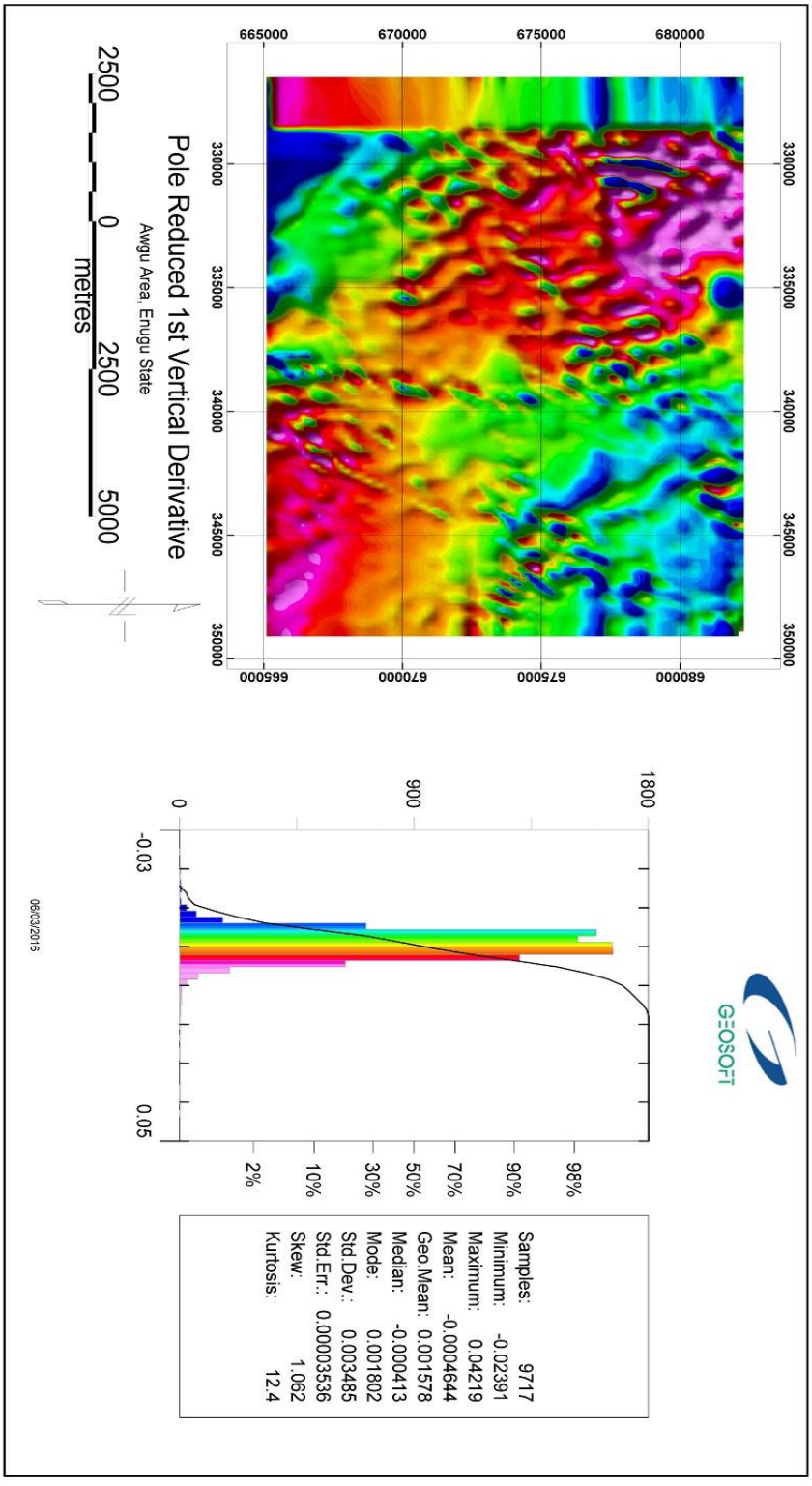

Figure 7. Reduction to pole.

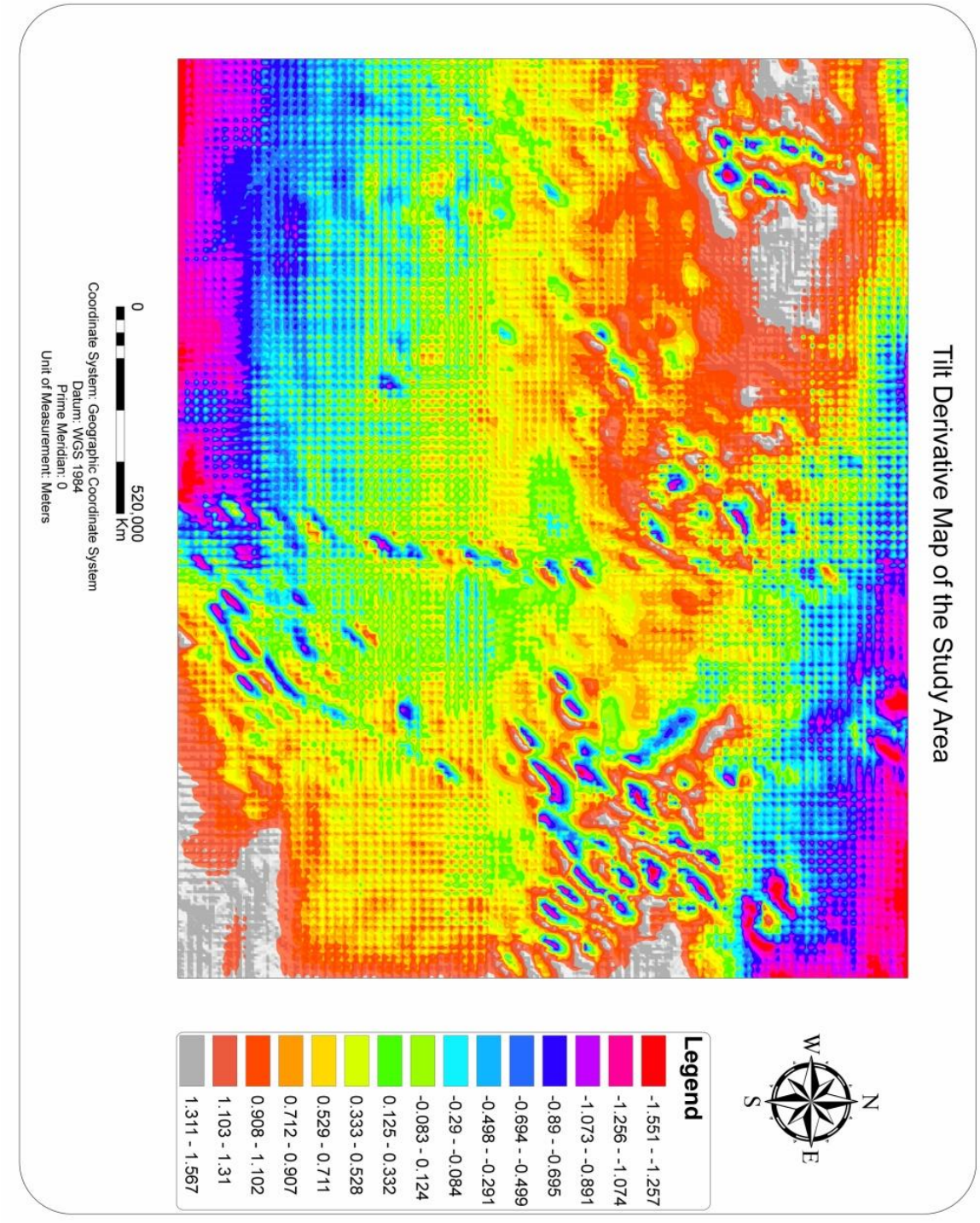

Figure 8. Tilt derivative.

.

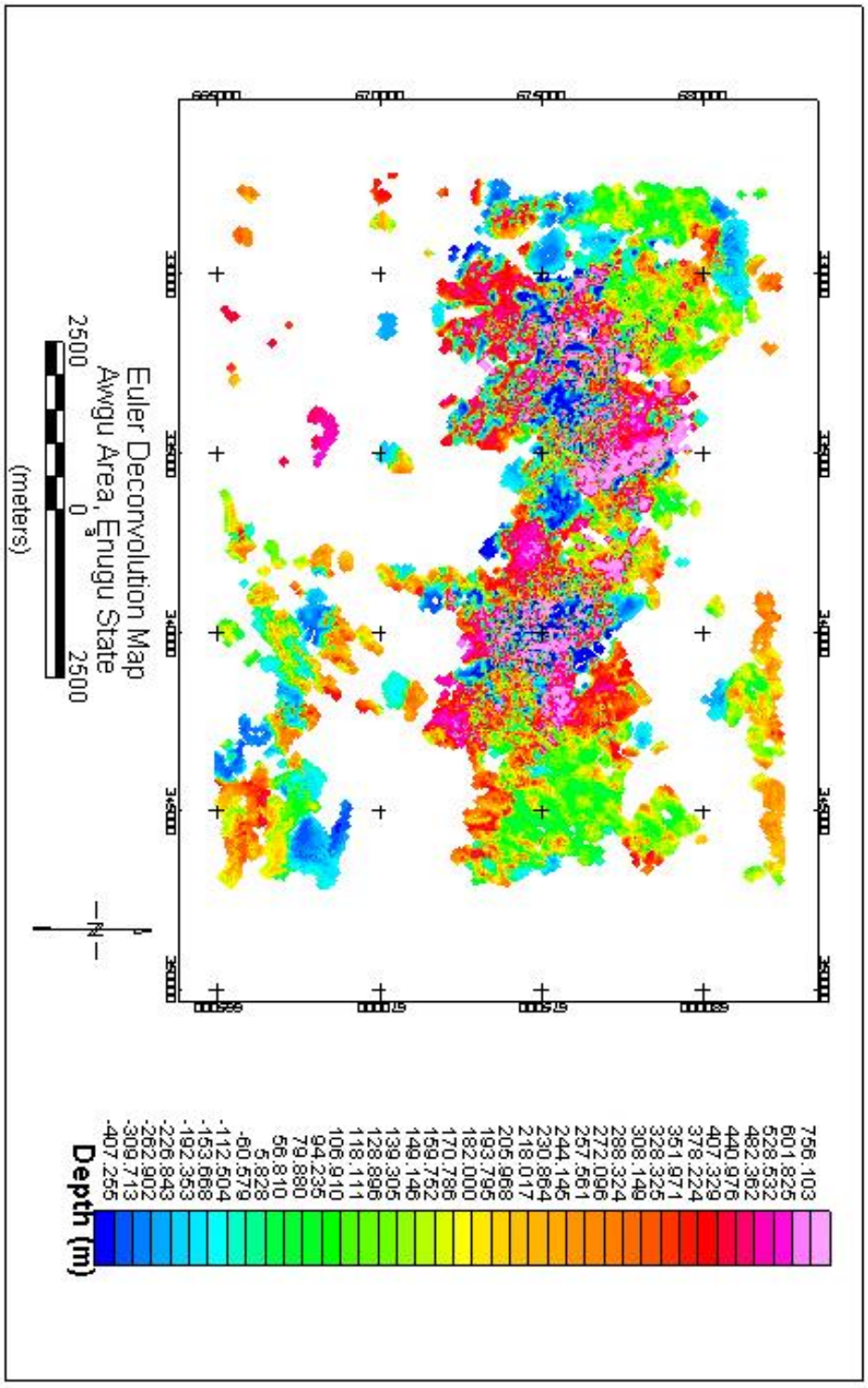

Figure 9. Euler deconvolution for structural index 1.0.

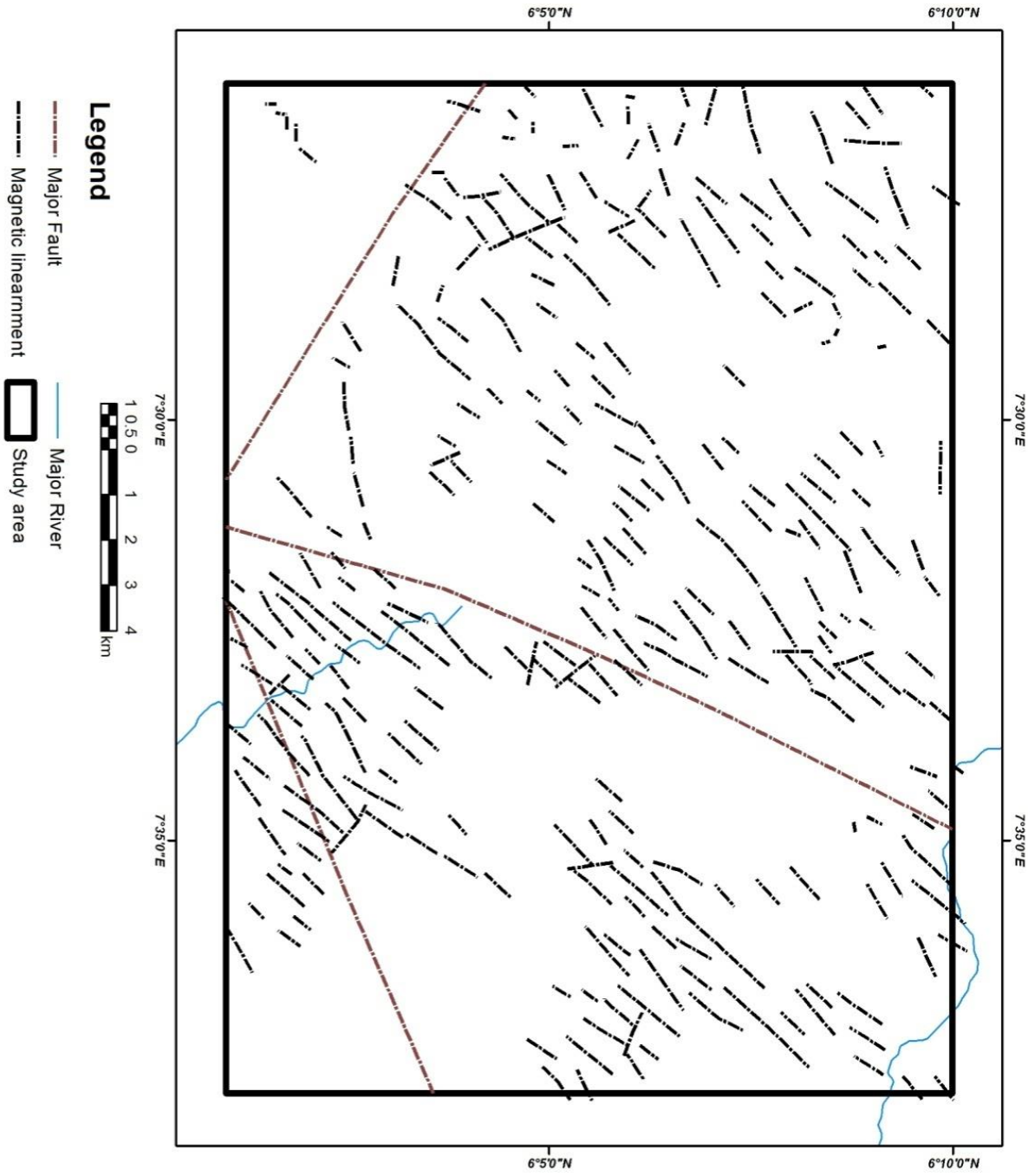

Figure 10. Aeromagnetic lineament map.

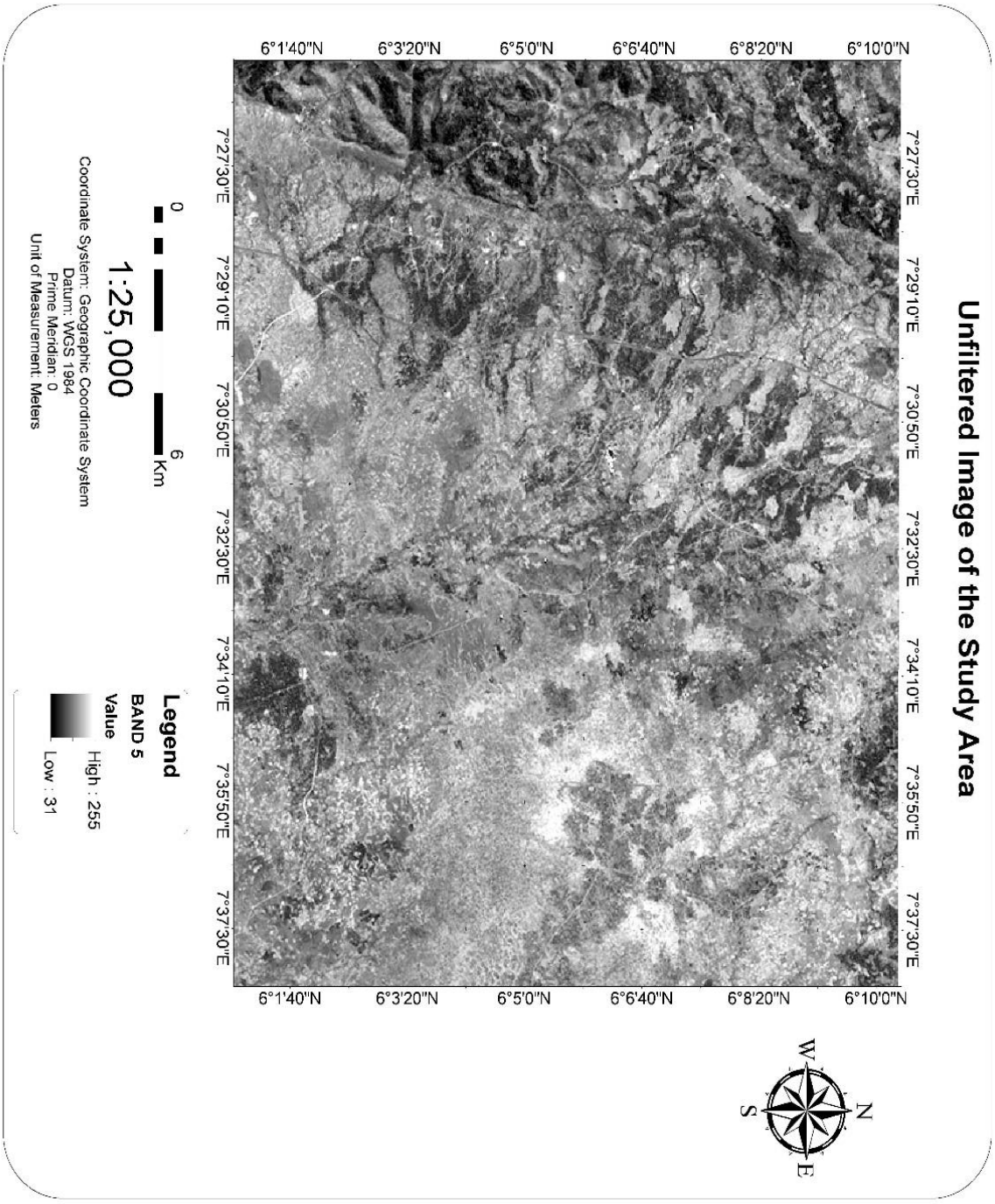

Figure 11a. Unfiltered image band 5 grey scale.

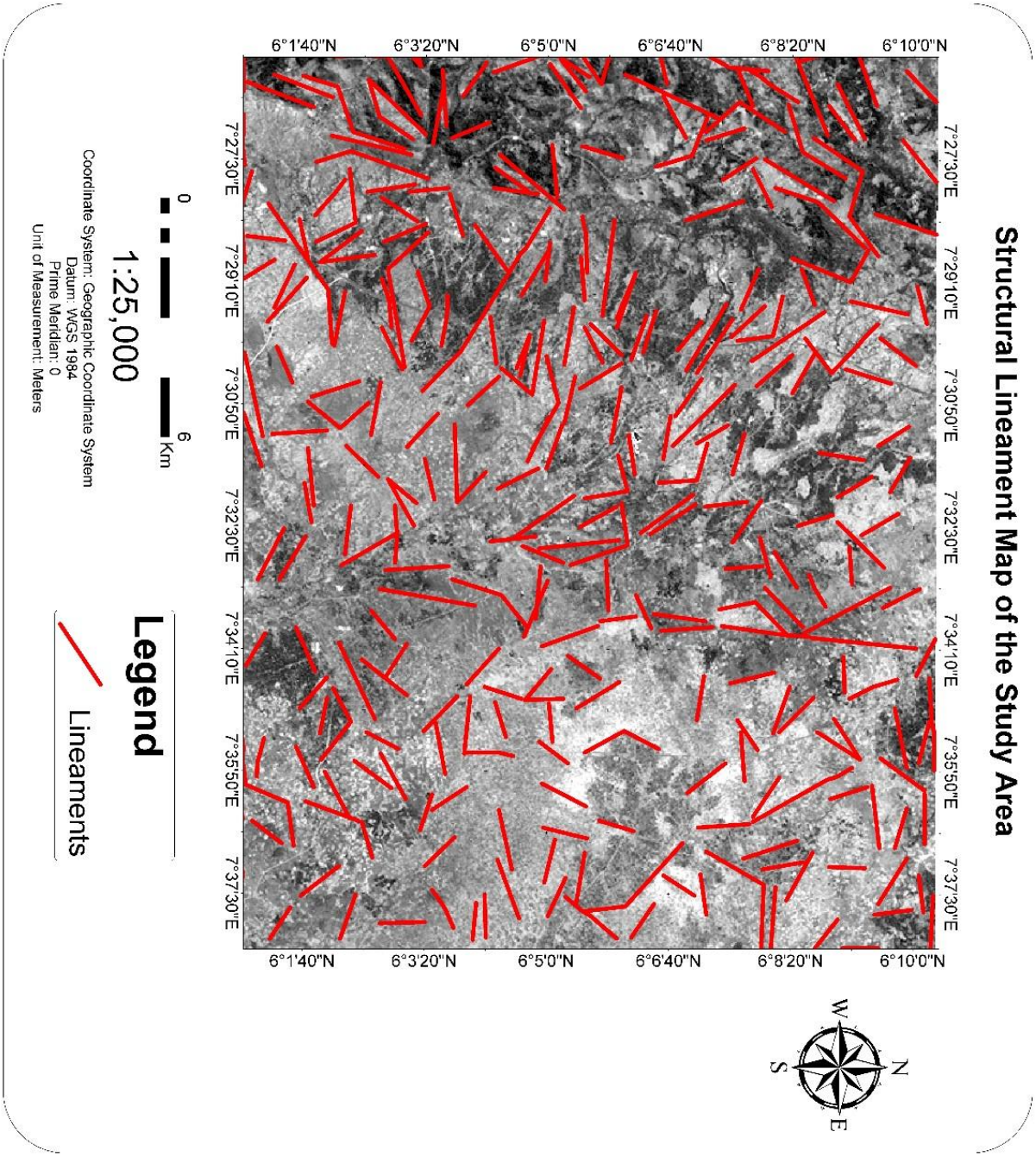

Figure 11b. Landsat lineaments ETM+ band 5

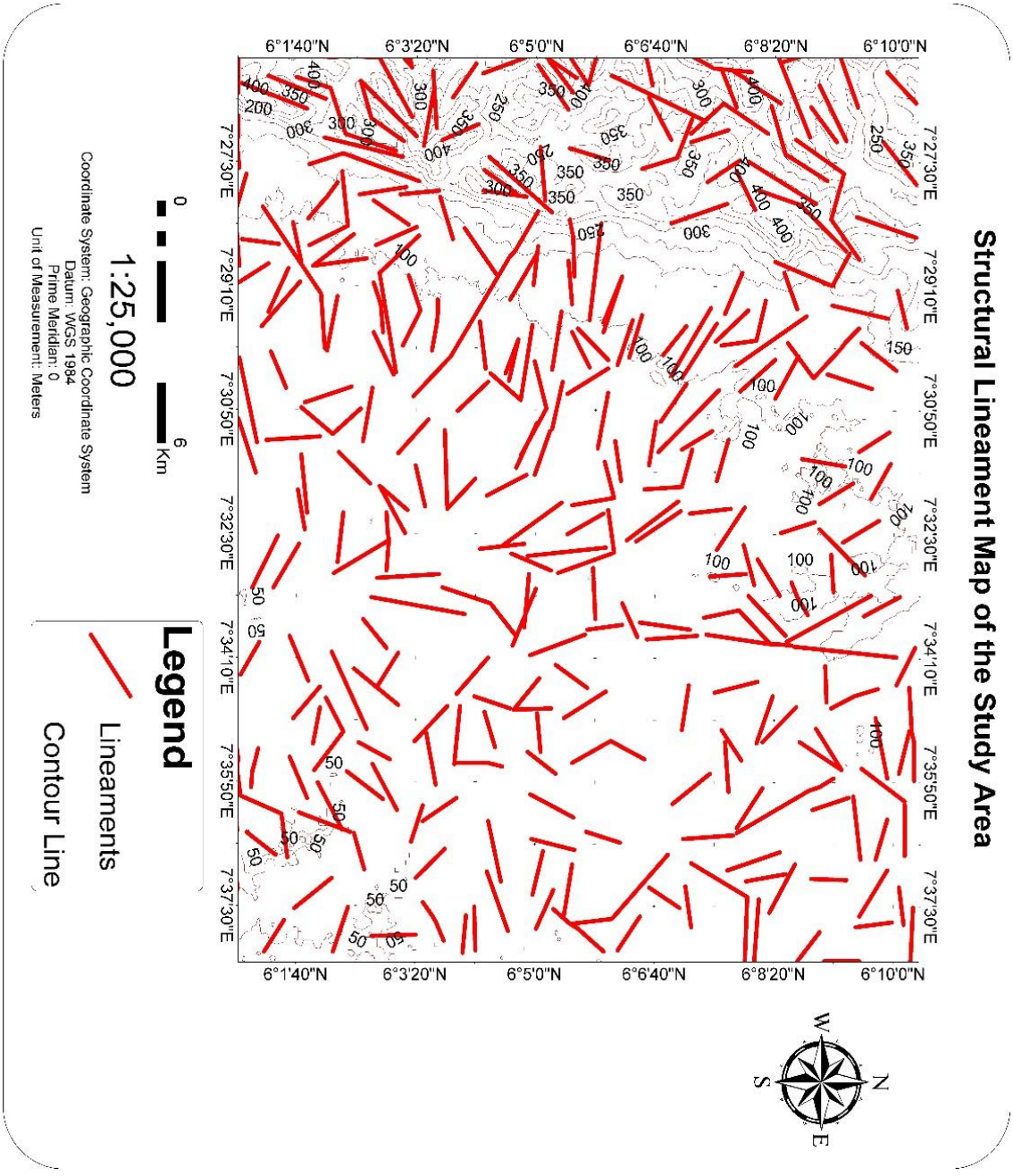

Figure 11c. Landsat lineaments contoured map.

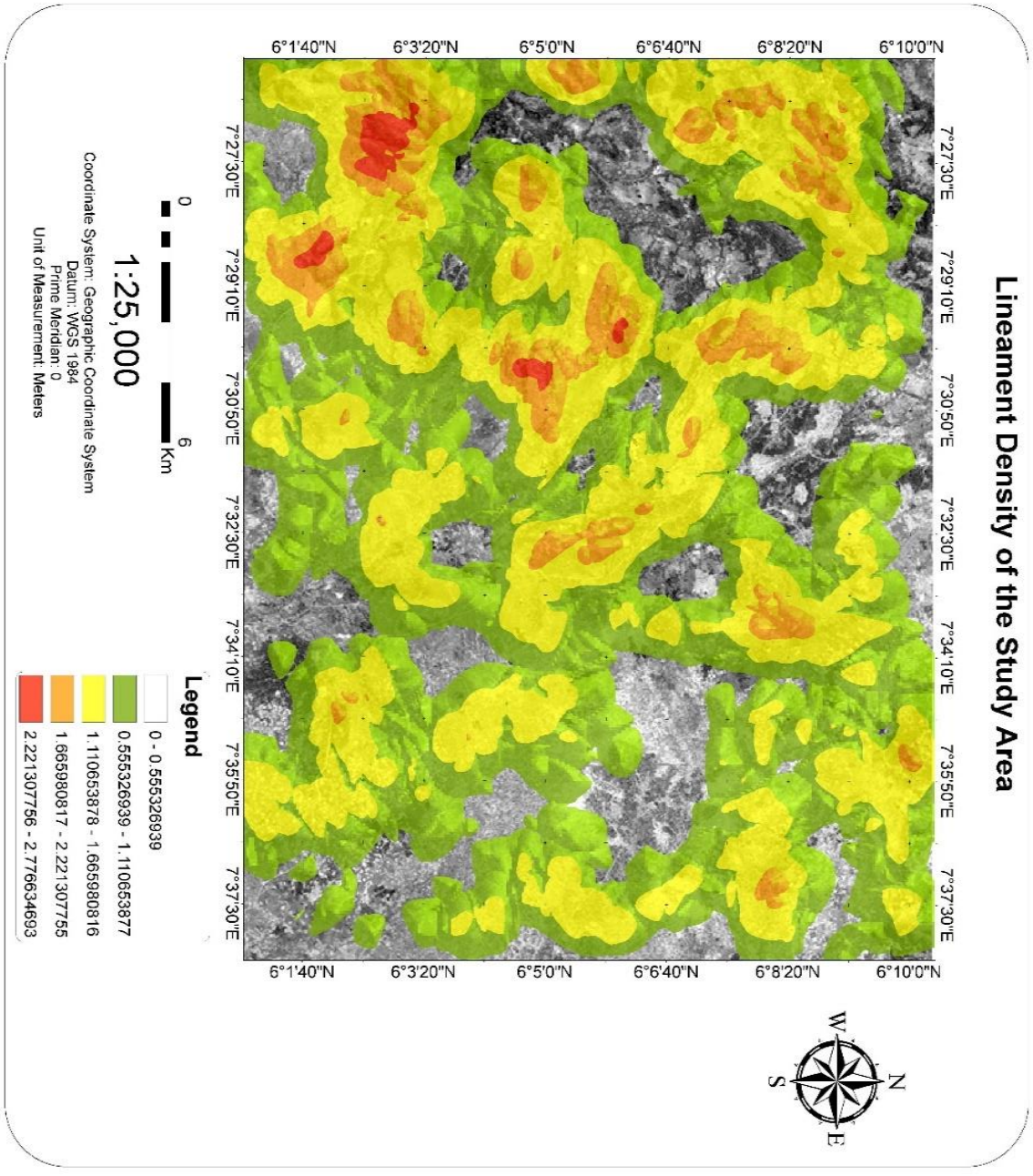

Figure 11d. Lineament density map of the study area.

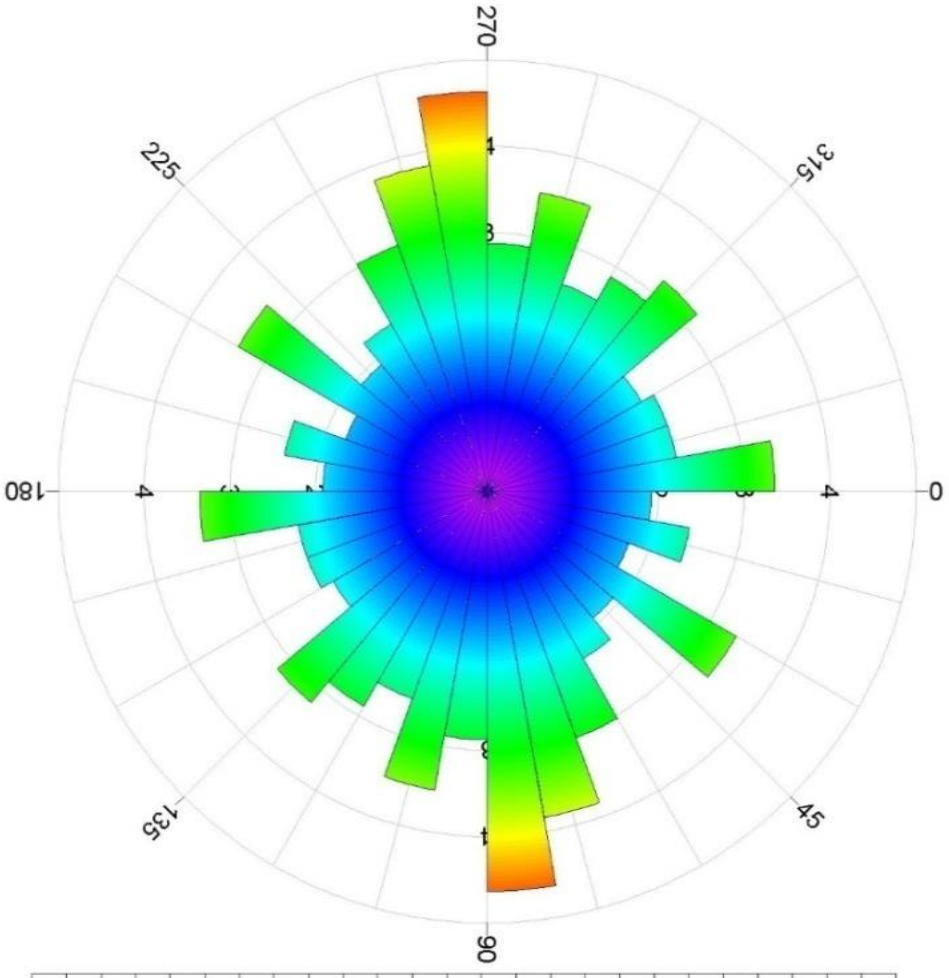

Rose Diagram

Statistical Summary

Calculation Method:	Frequency
Class Interval:	10.0 Degrees
Azimuth Filtering:	Deactivated
Data Type:	Bidirectional
Rotation Amount:	0.0 Degrees
Population:	313
Total Length of All Lineations:	626.0
Maximum Bin Population:	29.0
Mean Bin Population:	17.39
Standard Deviation of Bin Population:	4.76
Maximum Bin Population (%):	4.63
Mean Bin Population (%):	2.78
Standard Deviation of Bin Population (%):	0.76
Maximum Bin Length:	29.0
Mean Bin Length:	17.39
Standard Deviation of Bin Lengths:	4.76
Maximum Bin Length (%):	4.63
Mean Bin Length (%):	2.78
Standard Deviation of Bin Lengths (%):	0.76
Vector Mean:	92.0 Degrees
	272.04 Degrees
Confidence Interval:	40.4 Degrees
	(95 Percent)
R-mag:	0.11

Figure 12a. Landsat lineaments rose diagram.

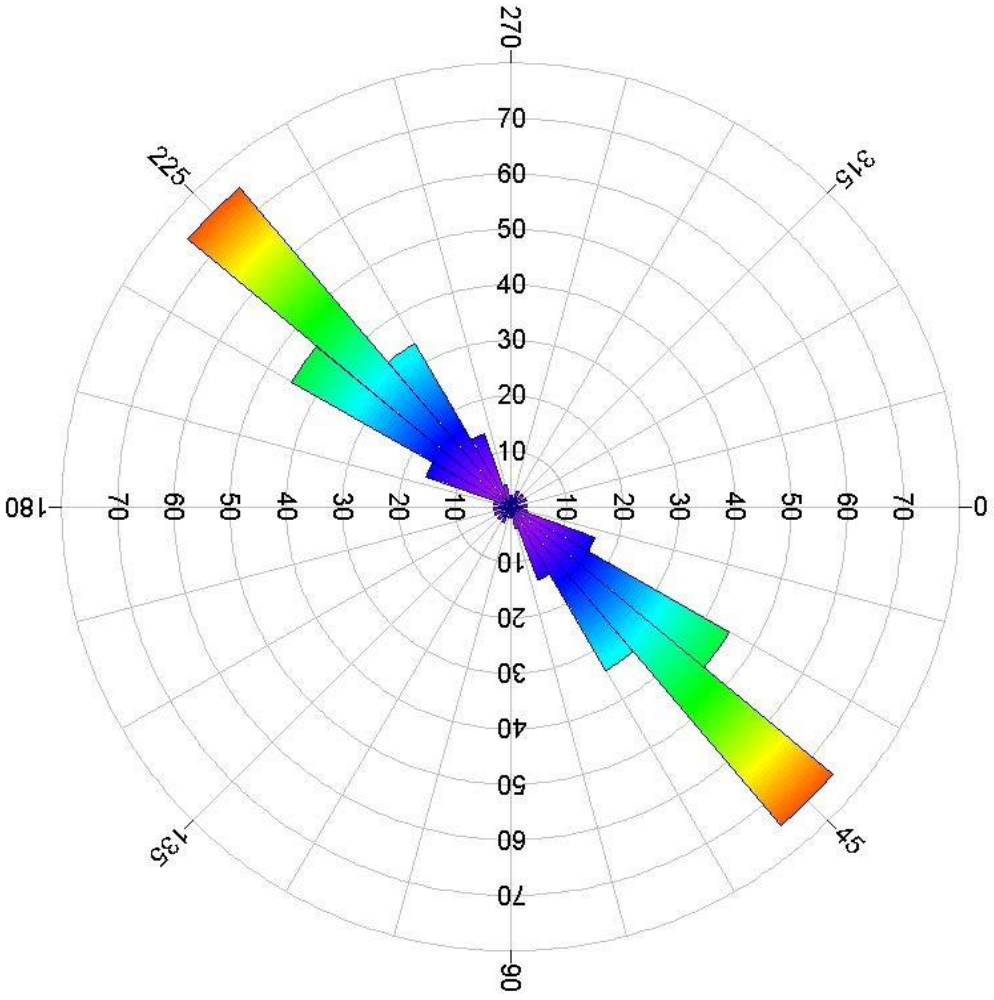

Rose Diagram

Statistical Summary

Calculation Method:	Frequency
Class Interval:	10.0 Degrees
Azimuth Filtering:	Deactivated
Data Type:	Bidirectional
Population:	211
Total Length of All Lineations:	422.0
Maximum Bin Population:	75.0
Mean Bin Population:	12.41
Standard Deviation of Bin Population:	20.17
Maximum Bin Population (%):	17.77
Mean Bin Population (%):	2.94
Standard Deviation of Bin Population (%):	4.78
Maximum Bin Length:	75.0
Mean Bin Length:	12.41
Standard Deviation of Bin Lengths:	20.17
Maximum Bin Length (%):	17.77
Mean Bin Length (%):	2.94
Standard Deviation of Bin Lengths (%):	4.78
Vector Mean:	43.7 Degrees
	223.7 Degrees
Confidence Interval:	5.3 Degrees
	(95 Percent)
R-mag:	0.79

Figure 12b. Aeromagnetic lineaments rose diagram.